Conducting Polymer/SWCNTs Modular Hybrid Materials via Diels–Alder Ligation

ARTICLE *in* MACROMOLECULES · APRIL 2013

Impact Factor: 5.8 · DOI: 10.1021/Ma4004055

Macromolecules

Article

pubs.acs.org/Macromolecules

Conducting Polymer/SWCNTs Modular Hybrid Materials via Diels–Alder Ligation

Basit Yameen,[†] Nicolas Zydziak,[†,‡] Steffen M. Weidner,[§] Michael Bruns,[ξ] and Christopher Barner-Kowollik[†,*]

[†]Preparative Macromolecular Chemistry, Institut für Technische Chemie und Polymerchemie, Karlsruhe Institute of Technology (KIT), Engesserstrasse 18, 76128 Karlsruhe, Germany

[‡]Polymer Engineering, Fraunhofer Institut für Chemische Technologie (ICT), Josef-von-Fraunhoferstrasse 7, 76327 Pfinztal (Berghausen), Germany

[ξ]Institute for Applied Materials (IAM) and Karlsruhe Nano Micro Facility (KNMF), Karlsruhe Institute of Technology (KIT), Hermann-von-Helmholtz-Platz 1, 76344 Eggenstein-Leopoldshafen, Germany

[§]BAM-Federal Institute for Materials Research and Testing, Richard-Willstätter-Straße 11, 12489 Berlin, Germany

Supporting Information

ABSTRACT: The development of a facile covalent strategy for the fabrication of organic conducting polymers (OCPs)/carbon nanotubes (CNTs) based molecular hybrid materials remains a challenge and is expected to address the detrimental intrinsic bundling issue of CNTs. In view of the pristine CNTs' ability to undergo Diels–Alder reactions with dienes, we report the synthesis of a novel poly(3-hexylthiophene) (P3HT) based organic conducting polymer (OCP) with terminal cyclopentadienyl (Cp) groups. The synthetic strategy employed is based on a combination of *in situ* end group functionalization via Grignard metathesis (GRIM) polymerization and a subsequent end group switching via reaction with nickelocene. Characterization data from Matrix-assisted laser desorption-ionization time-of-flight mass spectrometry (MALDI–TOF MS) fully support the successful synthesis of monofunctional Cp-capped P3HT, which was found to be highly reactive toward dienophile end-capped polystyrene (PS). The Cp-capped P3HT was subsequently ligated to the surface of pristine single walled CNTs (SWCNTs). The resulting P3HT/SWCNTs molecular hybrid material was characterized using thermogravimetric analysis (TGA), elemental analysis (EA), X-ray photoelectron spectroscopy (XPS), and high resolution transmission electron microscopy (HRTEM). The data from TGA, EA, and XPS were used to quantitatively deduce the grafting density. P3HT/SWCNTs prepared with Cp capped P3HT was found to contain 2 times more P3HT than the reference sample, featuring a grafting density of 0.0510 chains·nm^{-2} and a periodicity of 1 P3HT chain per 748 carbon atoms of the SWCNTs. HRTEM revealed individual SWCNTs wrapped with P3HT whereas in the reference sample P3HT was adsorbed on the bundles of the SWCNTs. The results presented here provide a new avenue for designing novel materials based on CNTs and OCPs.

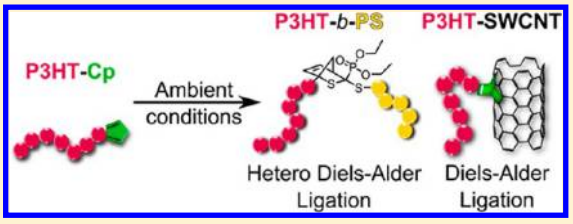

INTRODUCTION

Carbon nanotubes (CNTs) possess a unique set of optical, electrical, thermal, and mechanical properties which makes them versatile materials for applications in a variety of fields ranging from optoelectronics to biology.[1] However, the intrinsic tendency of CNTs to form bundles, induced by strong van der Waals interaction,[2] has been detrimental to their potential and a limiting factor for uses in a variety of new applications.[3] Significant efforts focused on addressing the bundling issue have suggested the CNTs surface chemical functionalization as a key to overcoming this obstacle and to benefit from the properties of such a technologically important material.[4] Organic optolectronics/solar cells,[5] offering low cost, easy to process, lightweight, flexible, reliable and environmentally benign energy production technology, is one area where the optoelectronic properties of CNTs are set to play a vital role.[6] On the other hand, the development of conducting polymers for electronic and photovoltaic devices is being extensively explored.[7] These semiconductor devices function based on the photovoltaic effect which involves the generation of excitons (electron–hole pairs) after photon absorption and their dissociation for current collection. In conducting polymers the excitons are short-lived and tend to recombine before the charge collection at the electrodes.[8] The dissociation of excitons can be promoted at the interface of a heterojunction between semiconductor materials of different electron affinities.[9] Conducting polymers (electron donor, D) and fullerenes (electron acceptor, A) are extensively employed to generate a heterojunction.[10] However, the desired optimum morphology for the active layer of the photovoltaic cells is predicted to be an interpenetrating network containing

Received: February 25, 2013
Published: March 28, 2013

   dx.doi.org/10.1021/ma4004055 | Macromolecules 2013, 46, 2606–2615

vertically aligned domains carrying the charges to the electrodes,[11] making CNTs a natural choice and holding promise for improving the photovoltaic effects. On the part of conducting polymers a highly fluorescent poly(3-hexyl)-thiophene (P3HT) is one of the most widely studied materials in the context of conducting polymers/CNTs bulk heterojunction (BHJ) systems. Several studies in recent years have predicted an improvement of charge separation efficiency for P3HT/CNTs based BHJ systems as compared to fullerene based systems.[12] However, this improvement remained naturally connected to the debundling of CNTs allowing a better contact between P3HT (D) and the CNTs (A) surface. A rationally designed surface functionalization of CNTs is key to provide the required BHJ systems. Both noncovalent supramolecular interaction and covalent functionalization are being explored. The noncovalent CNTs surface functionalization strategies exploit the van der Waals/$\pi-\pi$ interactions[13] resulting in physical adsorption of conducting polymers at the surface of CNTs, whereas the covalent functionalization strategies exploit various surface chemical reactions to covalently graft chemical moieties at the surface of CNTs.[4,6] Because of its chemical robustness, covalent functionalization is generally preferred over noncovalent adsorption which is prone to desorption under stress. Kuila et al.[14] have reported an improved photovoltaic cell performance when P3HT was covalently functionalized at the surface of the CNTs. Similarly, the studies of Kumar et al.,[15] Boon,[16] Niu et al.,[17] Sadhu et al.,[18] and Phuong et al.[19] have reported improved photovoltaic characteristics achieved by the functionalization of CNT surfaces with P3HT. In all these examples the P3HT chains are grafted onto the surface of prefunctionalized CNTs via intricate, multistep prefunctionalization treatments, involving the oxidation of CNTs often under extremely aggressive conditions. Although a range of covalent strategies[20] have been explored to control the surface chemical nature of CNTs, there still exists a genuine challenge to develop facile and direct surface functionalization of pristine CNTs. In the context of surface functionalization and polymer−polymer ligation under ambient conditions our group has demonstrated the scope and promise of Diels−Alder reactions.[21] Recently, we have also demonstrated a facile Diels−Alder process for the direct surface functionalization of fullerenes and CNTs, where no surface pretreatment of the fullerenes or CNTs was necessary.[22] The scope of such cycloaddition reactions based surface modifications is striking: they are simple, work under ambient conditions, are applicable to all the graphitic carbon allotropes, and do not need any surface pretreatment or catalyst. Despite of some important reports highlighting theoretical as well as practical viability of Diels−Alder reaction for the CNTs surface functionalization,[23] this important and highly promising avenue is yet to be explored for ligating well-defined conducting macromolecules to the surface of CNTs. Thus, the aim of the present work is to design an unprecedented conducting polymer with a highly reactive diene end-group (i.e., cyclopentadienyl, Cp) suitable for subsequent direct ligation with nonmodified single walled carbon nanotubes (SWCNTs). We have achieved the above goal by synthesizing novel Cp end-capped P3HT via an *in situ* chain end-capping strategy developed by McCullough and coworkers[24] The Cp end-capped P3HT was fully characterized employing NMR spectroscopy and MALDI−TOF MS. The reactivity of the Cp end groups was demonstrated by synthesizing P3HT-*b*-PS block copolymers via hetero Diels−Alder (HDA) ligation. Exploiting the Diels−Alder reactivity of SWCNTs toward dienes, the new Cp end-capped P3HT was covalently grafted directly onto the surface of pristine SWCNTs and the resulting P3HT functionalized SWCNTs were fully characterized by X-ray photoelectron spectroscopy (XPS), elemental analysis (EA), thermogravimetric analysis (TGA), and high resolution transmission electron microscopy (HRTEM). The results reported here are of paramount importance on the one hand in the context of pioneering the synthetic design of Cp-capped conducting polymers which are highly suitable for Diels−Alder based modular ligation and on the other hand for the direct ligation of conducting polymer onto the surface of pristine SWCNTs. We believe the present report will introduce an important new aspect to the design of conducting polymer based materials.

EXPERIMENTAL SECTION

Synthesis of Aliphatic Bromo-Terminated P3HT (P−Br). A 540 mg sample of **P−OH** (0.085 mmol) was dissolved in 50 mL of dry THF and stirred at 40 °C for 15 min. To this solution 3.91 mL (28.05 mmol) of TEA were added followed by dropwise addition of 2.67 mL (25.5 mmol) of 2-bromopropionyl bromide at 40 °C. The reaction mixture was stirred at 40 °C for 24 h, after which it was cooled to ambient temperature and filtered. The filtrate was concentrated and precipitated in methanol. The precipitates were collected and subjected to Soxhlet extraction with methanol for 24 h. The **P−Br** was collected by extraction with chloroform and the chloroform was removed on a rotary evaporator. The obtained **P−Br** (M_n 6500 Da, $Đ$ 1.1) was subsequently dried under vacuum at ambient temperature.

Synthesis of Cp-Terminated P3HT (P−Cp). The synthesis of **P−Cp** was adapted from the method developed by Inglis et al.,[21h] and a representative synthesis is described here. The reaction was performed at ambient temperature in a glovebox under N_2(g) atmosphere. Then 527 mg (0.081 mmol) of **P−Br** (M_n, 6500 Da; PDI, 1.15) was dissolved in 21 mL of dry THF. To this solution 72.74 mg (0.485 mmol) NaI and 42.43 (0.162 mmol) of TPP were added, and the solution was stirred for 5 min. Then 61.11 mg (0.324 mmol) of $NiCp_2$ was separately dissolved in 1.8 mL of THF and was transferred to the solution of **P−Br** containing NaI and TPP. The reaction was stirred at ambient temperature for 6.5 h. The reaction mixture was subsequently passed through a short basic alumina column, concentrated, and precipitated in methanol. The precipitates were collected by centrifugation and were dissolved in chloroform. The chloroform mixture was washed three times with water, concentrated and precipitated in methanol. The precipitates were collected by centrifugation and dried overnight under vacuum at ambient temperature to give **P−Cp** (M_n 6500 Da, $Đ$ 1.2).

Synthesis of P3HT-*b*-PS via HDA Click Ligation. First, 24.8 mg (M_n 6500 Da, $Đ$ 1.2, 3.8×10^{-3} mmol) of **P−Cp**, 11.86 mg (M_n 3100 Da, $Đ$ 1.1, 3.8×10^{-3} mmol) of RAFT-polymerized **PS**, and 1.2 equiv of $ZnCl_2$ were dissolved in 70 μL of THF. The solution was stirred at 50 °C for 24 h. The reaction was cooled to ambient temperature and the polymer was recovered by precipitation in methanol. The obtained block copolymer was dissolved several times in the minimum volume of THF and precipitated in acetone. The precipitates were collected by centrifugation and dried under vacuum at ambient temperature.

Ligation of Cyclopentadienyl End-Capped P3HT with SWCNTs and Reference Sample (SWCNT-0 and SWCNT-1). First, 35 mg of pristine SWCNTs (**p-SWCNT**) was dispersed in 350 mL NMP in an ultrasonic bath with nitrogen purging for 1 h. Then, 350 mg of cyclopentadienyl end-capped P3HT (**P−Cp**) was added to the mixture and degassed for 15 min. The mixture was allowed to stir at ambient temperature for 24 h under inert atmosphere at 80 °C to generate the sample **SWCNT-1**. The reference sample (**SWCNT-0**) was prepared by mixing of SWCNTs and nonfunctional P3HT (**P-0**) under identical conditions.

dx.doi.org/10.1021/ma4004055 | *Macromolecules* 2013, 46, 2606−2615

Scheme 1. (A) Synthesis of Cp End-Capped P3HT (P−Cp) by a Combination of *in Situ* End-Functionalization Employing GRIM Polymerization and $NiCp_2$-Assisted Transformation of the Terminal Aliphatic Bromo Group into a Cp Group[a] and (B) Synthesis of a Reference P3HT Sample (P-0)[b]

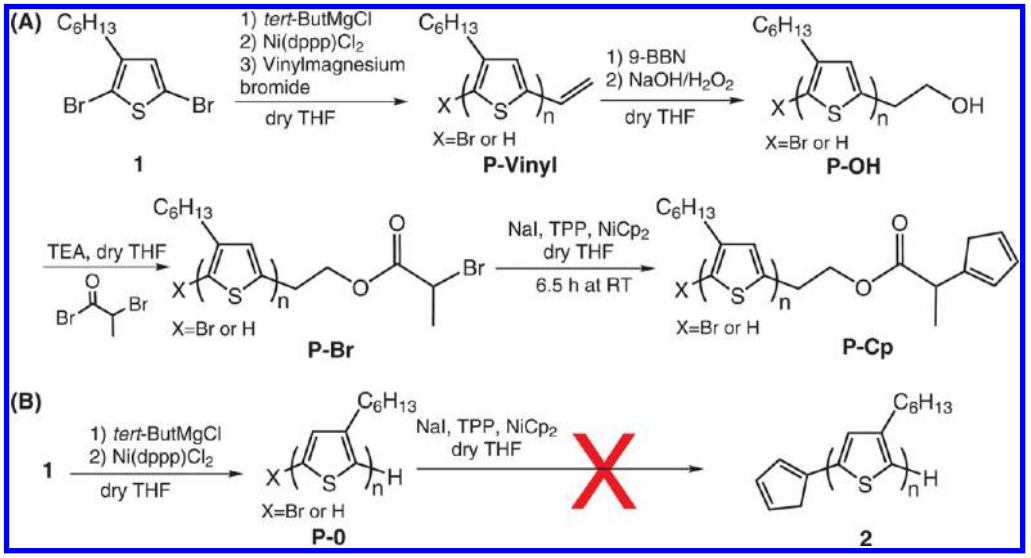

[a]The transformation produces a mixture of 1-, 2-, and 5-substituted cyclopentadienes; only the 1-isomer is presented for reasons of brevity. [b]The terminal bromo groups of the **P-0** remained inert during reaction with $NiCp_2$.

RESULTS AND DISCUSSION

Synthesis of Cp End-Capped P3HT. The synthetic strategy employed to generate the Cp capped P3HT conducting polymer was based on the *in situ* end functionalization using the Grignard metathesis (GRIM) polymerization developed by McCullough and coworkers[24] The GRIM method generally yields regio-regular head-to-tail coupled P3HT with a predominant chain end composition of H/Br. Exploiting the chain growth mechanism of GRIM polymerization McCullough and colleagues have further developed a simple route to various end-capped P3HT polymers simply by adding a pertinent Grignard reagent (RMgX), leading to P3HT with a predominant chain end composition of Br/R with a small fraction of an H/R combination. In the present study (refer to Scheme 1), we prepared P3HT with a Br/Vinyl chain end combination (**P-Vinyl**) by adding vinylmagnesium bromide at the end of the polymerization. The terminal vinyl groups were transformed into hydroxyl ethyl groups by subjecting them to hydroboration using 9-BBN followed by oxidation with H_2O_2 in the presence of NaOH. The hydroxyl end-capped P3HT was subsequently reacted with 2-bromopropionyl bromide to give **P−Br** with a chain end constitution of aromatic-Br/aliphatic-Br.[24a] Capitalizing on the $NiCp_2$ assisted ambient temperature transformation of aliphatic bromo to Cp groups,[21h] the terminal aliphatic-Br groups of **P−Br** were quantitatively transformed into the Cp groups (Scheme 1A; although the transformation leads to a mixture of 1-, 2-, and 5-substituted cyclopentadienes, only the chemical structure for the 1-isomer is presented for reasons of brevity). For the sake of comparison, a P3HT polymer with a chain end constitution of Br/H (**P-0**) was additionally prepared employing the same GRIM method (Scheme 1B). The ^{1}H NMR and MALDI−TOF MS spectra for **P-0** are provided in Figures S2 and S3 in the Supporting Information section.

Characterization of the Synthesized Polymers. All end group transformations were characterized by ^{1}H NMR spectroscopy and MALDI−TOF MS. The ^{1}H NMR data for the transformation steps leading to the **P−Br** stage were in complete agreement with those reported in the literature[24a] (refer to Figure S1 in the Supporting Information section for the ^{1}H NMR spectra of **P-Vinyl** and **P−OH**). The successful transformation of aliphatic-Br of **P−Br** to Cp end groups was evidenced by the appearance of proton resonances characteristics for the Cp group[21h] at 6.0−6.5 and 2.9 ppm in the ^{1}H NMR spectrum of **P−Cp**. The resonance for the proton at the α-position to the aliphatic−Br group was also shifted from 4.3 ppm in **P−Br** to 3.5 ppm in **P−Cp**. Additionally, the doublet for the methyl protons at β-position to the aliphatic−Br group was shifted upfield, being obscured by the aliphatic signals from the hexyl substituents of P3HT. The ^{1}H NMR data thus fully corroborate the successful end group transformation (refer to Figure 1). The presence of distinguishable end groups enabled the estimation of M_n values by the ^{1}H NMR end group analysis. The consistent M_n values of **P-Vin** (7800 Da), **P−OH** (8100 Da), **P−Br** (8000 Da), and **P−Cp** (8600 Da) reflect on a high end group fidelity during the end group transformation depicted in Scheme 1.

In addition to ^{1}H NMR spectroscopy, MALDI−TOF MS analysis also confirms the quantitative end group transformation. The MALDI−TOF MS spectra of **P-Vinyl**, **P−OH**, and **P−Br** are provided in the Supporting Information section (refer to Figure S4). The MALDI−TOF MS spectrum for the **P−Cp** is depicted in the Figure 2. The m/z values for the major peak series in Figure 2 correspond to the **P−Cp** molecules as expected (refer to Scheme 1) with a Cp group at one end of the chain, while the other end of the chain is capped with the bromo group. It is worthwhile noting that only the aliphatic-Br end groups of **P−Br** were transformed into the Cp groups while the bromo groups directly attached to the thiophene ring did not react with the $NiCp_2$. The transformation of the bromo end groups of the **P-0** (M_n 4000 Da, $Đ$ 1.1) into a Cp group under similar conditions did not occur (product **2**, with m/z 2059, in Scheme 1B is not observed, refer to Figure S5 in the Supporting Information section), which

dx.doi.org/10.1021/ma4004055 | *Macromolecules* 2013, 46, 2606−2615

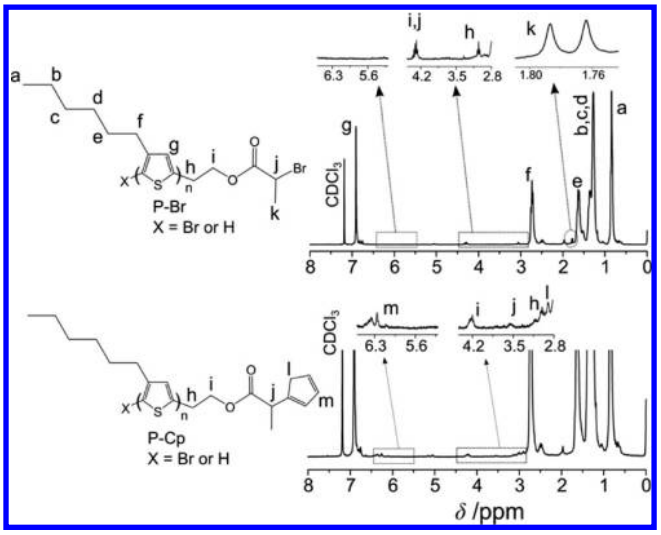

Figure 1. ^{1}H NMR spectra of **P−Br** (top) and **P−Cp** (bottom) with resonance assignment to the respective protons revealing the successful transformation of the terminal aliphatic bromo group into a Cp group.

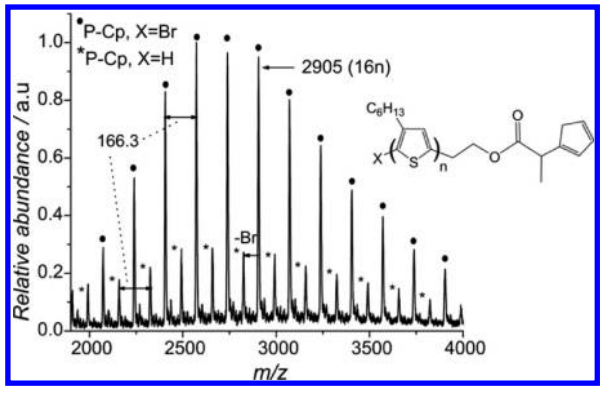

Figure 2. MALDI−TOF MS spectrum of **P−Cp**. The major peak series corresponds to **P−Cp** with X = Br while the minor peak series represents **P−Cp** with X = H. For both series the difference between two consecutive peaks matches the mass of P3HT repeat units. For a detailed peak assignment, refer to Table 1.

evidence the inertness of bromo groups directly attached to thiophene rings toward $NiCp_2$ under the applied condition. In the MALDI−TOF mass spectrum of **P−Cp**, as depicted in Figure 2, the difference of 166.3 Da between the consecutive major peaks (marked with a point •) matches the mass of P3HT repeat units well. In addition to the major peak series a minor peak series, as marked by the asterisks in Figure 2, was also observed. A difference of 166.3 Da between the consecutive minor peaks confirmed that they are also originated from P3HT molecules and the mass difference between the consecutive minor and major peaks matched the mass of a bromine atom which reflected on the **P−Cp** molecules with H/Cp chain ends constitution. This is in accord with the results reported by the McCullough et al., where quenching the GRIM polymerization with vinylmagnesium bromide results in P3HT with a majority chain end constitution of Br/Vinyl and a minor fraction of H/Vinyl chain end constitution.[24] The combination of chain ends is subsequently carried over into all the end group transformations as depicted in Scheme 1A.

A comparison of MALDI−TOF mass spectra of **P−Br** and **P−Cp** is presented in Figure 3 along with the chemical

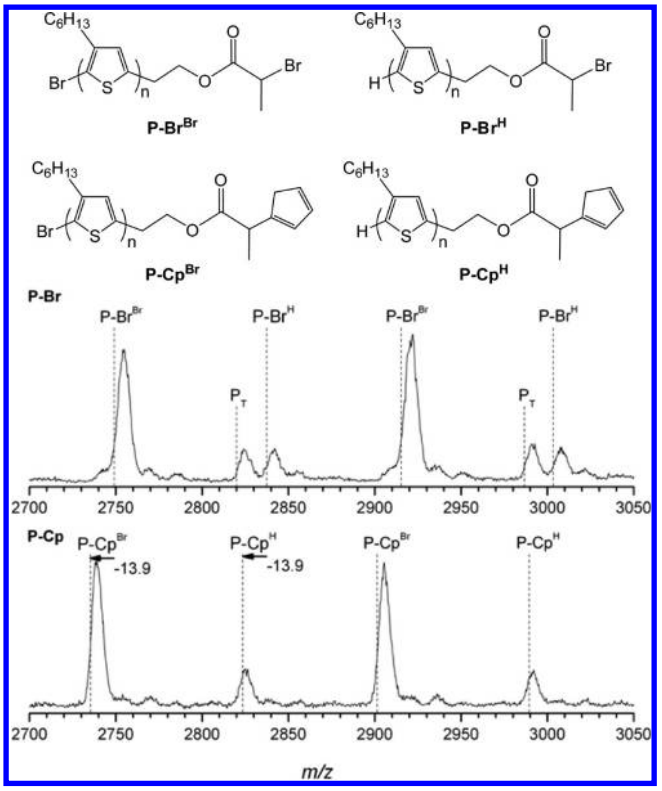

Figure 3. Top: Chemical structures of the **P−Br** (**P−Br^{Br}** refers to Br/Br and **P−Br^{H}** refers to H/Br chain end constitution) and **P−Cp** (**P−Cp^{Br}** refers to Br/Cp and **P−Cp^{H}** refers to H/Cp chain end constitution) polymers. Bottom: MALDI−TOF MS spectra of **P−Br** and **P−Cp**. A shift of peaks by −13.88 Da (78.92 (Br) − 65.04 (C_5H_5) = 13.88 Da) confirms the quantitative transformation of the terminal aliphatic bromo group to a Cp group.

structures of the **P−Br** (**P−Br^{Br}** refers to Br/Br and **P−Br^{H}** refers to H/Br chain end constitution) and **P−Cp** (**P−Cp^{Br}** refers to Br/Cp and **P−Cp^{H}** refers to H/Cp chain end constitution) polymers. The absence of **P−Br^{Br}** species in the **P−Cp** MALDI−TOF mass spectrum and a shift of the peaks by −13.9 Da (78.92 (Br) − 65.04 (C_5H_5) = 13.88 Da) confirmed the quantitative transformation of only the terminal aliphatic bromo groups of **P−Br^{Br}**, into Cp groups. The transformation is clearly observable for **P−Br^{Br}** species, however, in the case of the transformation of the **P−Br^{H}** species, the **P−Cp^{H}** peaks overlaps with a small peak (marked as P_T) already present in the **P−Br** mass spectrum in the same region. A 166.3 Da difference between consecutive P_T peaks shows their origin from the P3HT; however, the exact end group nature of the P_T is unclear at this stage. Nevertheless, one can clearly observe the disappearance of the **P−Br^{H}** peaks, confirming the quantitative transformation. Furthermore, the peak shift of −13.9 Da during the transformation of **P−Br** to **P−Cp** confirms the inertness of the bromo group which is directly attached to the thiophene ring toward the $NiCp_2$ transformation procedure under the applied conditions. The MALDI−TOF MS data for **P−Br** and **P−Cp** are summarized in Table 1. A close agreement between the theoretical and the experimental *m*/*z* values fully corroborates the chain end constitution (refer to Figures S6 and S7 in the Supporting Information, showing close agreement between the experimentally measured MALDI−TOF MS and the simulated mass spectra for **P−Br** and **P−Cp**). To avoid any interference from

dx.doi.org/10.1021/ma4004055 | *Macromolecules* 2013, 46, 2606−2615

Table 1. Summary of MALDI–TOF MS Data for Different Chain End Constitutions of P–Br and P–Cp[a]

species	n	formula	m/z theor	m/z expt	$\Delta m/z$
P–Br^{Br}	15	$[C_{155}H_{218}Br_2O_2S_{15}]^+$	2749.11	2749.41	0.30
P–Br^{H}	16	$[C_{165}H_{233}BrO_2S_{16}]^+$	2837.28	2837.63	0.35
P–Br^{Br}	16	$[C_{165}H_{232}Br_2O_2S_{16}]^+$	2915.20	2915.30	0.1
P–Br^{H}	17	$[C_{175}H_{247}BrO_2S_{17}]^+$	3003.37	3003.77	0.40
P–Cp^{H}	15	$[C_{160}H_{223}BrO_2S_{15}]^+$	2735.23	2735.27	0.04
P–Cp^{Br}	16	$[C_{170}H_{238}O_2S_{16}]^+$	2823.41	2823.59	0.18
P–Cp^{H}	16	$[C_{170}H_{237}BrO_2S_{16}]^+$	2901.32	2901.40	0.08
P–Cp^{Br}	17	$[C_{180}H_{252}O_2S_{17}]^+$	2989.49	2988.99	0.50

[a] n represents the number of monomer repeat units.

P_T and considering the quantitative nature of the **P–Br** to **P–Cp** transformation, the end group fidelity was estimated at the **P–Br** stage. A comparison of the area under the peaks associated with **P–Br^{Br}**, **P–Br^{H}**, and P_T in the MALDI–TOF mass spectrum of **P–Br** revealed an end group fidelity of 90%. These data—jointly with the NMR data—evidence the efficacy of our synthetic approach for the introduction of a Cp unit at the terminus of a P3HT chain.

An overlay of the GPC traces of **P–Br** and **P–Cp** is depicted in Figure 4. The two chromatograms are essentially identical

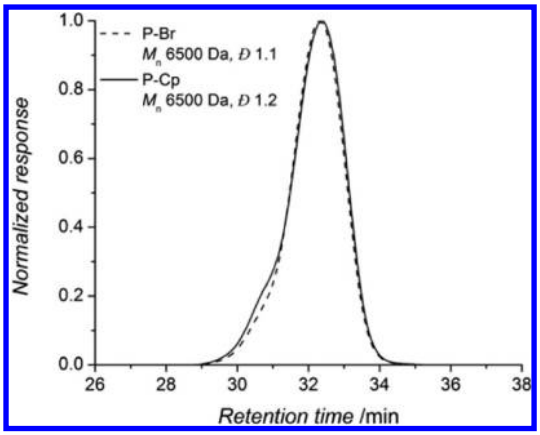

Figure 4. Overlay of GPC traces of **P–Br** and **P–Cp**.

except a very small shoulder that appeared on the higher molecular weight side for **P–Cp**. The small shoulder can be attributed to a Diels–Alder coupling reaction between the Cp end groups of **P–Cp**. The overall GPC data for **P–Br** (M_n 6500 Da, Đ 1.1) and **P–Cp** (M_n 6500 Da, Đ 1.2) are almost identical, and both of the polymers have narrow dispersities.

Synthesis of P3HT-*b*-PS via HDA Ligation. After characterizing the **P–Cp** polymer and ascertaining the nature of the end groups, the reactivity of the Cp end groups as a diene in a Diels–Alder reaction was demonstrated. For this purpose, **PS** carrying dithioester based electron deficient dienophile end groups was synthesized by employing benzyl (diethoxyphosphoryl)dithioformate as chain transfer agent according to the RAFT procedure previously established by our group.[21a] The suitability of electron-deficient dithioester end-capped polymers for block copolymer synthesis via [4 + 2] HDA cycloaddition reactions has been previously established.[21] The HDA cycloaddition coupling reaction was performed between Cp (diene) end-capped P3HT **P–Cp** and RAFT polymerized electron deficient dithioester (dienophile) end-capped **PS** (refer to Scheme 2). The reaction was performed in THF in the presence of $ZnCl_2$ at 50 °C for 24 h.

The GPC analysis of the reaction mixture clearly showed the formation of the block copolymer. The corresponding GPC traces of the initial polymers and the formed block copolymer are depicted in Figure 5 and their molecular weights are collated in Table 2.

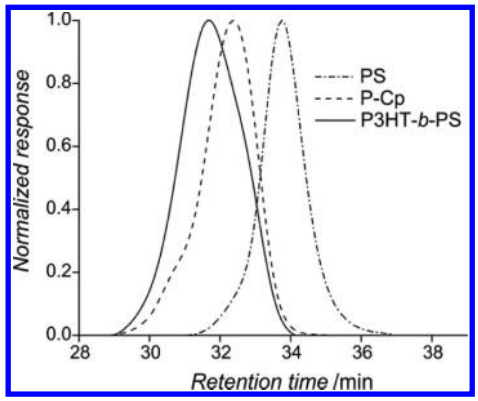

Figure 5. Overlay of GPC traces of **P–Cp**, RAFT-synthesized **PS** with dithioester end groups, and **P3HT-*b*-PS** synthesized via HDA ligation.

Table 2. GPC Data for the P–Cp, RAFT-Synthesized PS with Dithioester End Groups, P3HT-*b*-PS Synthesized via HDA Ligation, and Reference P3HT P-0 Polymer Samples

sample	M_p (Da)	M_n (Da)	M_w (Da)	Đ
P–Cp	6300	6500	7600	1.2
PS	3300	3100	3500	1.1
P3HT-*b*-PS	8700	7800	9100	1.2
P-0	6100	6200	6800	1.1

The resulting block copolymer was also characterized by ^{1}H NMR spectroscopy. Before ^{1}H NMR spectroscopic analysis, the block copolymer sample was repeatedly precipitated from its THF solution into acetone. Such a procedure removed any traces of unreacted **PS** which is readily soluble in acetone (refer to Figure S13 in the Supporting Information section). The ^{1}H NMR spectrum of the purified **P3HT-*b*-PS** formed by the [4+2] HDA cycloaddition reaction clearly showed the signals for the aromatic proton resonances originating from the **PS** block (refer to Figure S8 in the Supporting Information

Scheme 2. Schematic Representation of the P3HT-*b*-PS Synthesis via HDA Ligation

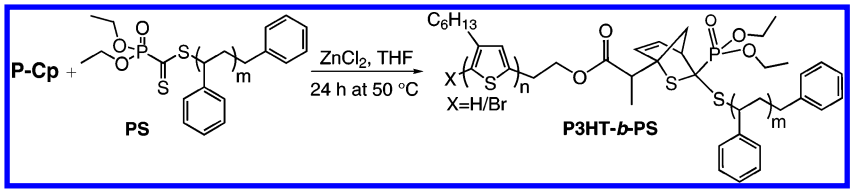

dx.doi.org/10.1021/ma4004055 | Macromolecules 2013, 46, 2606–2615

section). These results support the suitability of the terminal Cp groups of **P−Cp** to undergo Diels−Alder reactions.

Ligation of Cp End-Capped P3HT with SWCNTs. The so far discussed characterization data for the **P−Cp** augmented by the example of block copolymer formation clearly evidence the presence of Diels−Alder-active Cp groups at the end of P3HT chains. The **P−Cp** was subsequently reacted with pristine SWCNTs (**SWCNT-1**) in order to demonstrate the unprecedented one-step facile and direct surface functionalization of pristine SWCNTs with P3HT via Diels−Alder ligation. The surface Diels−Alder ligation was carried out at 80 °C for 24 h. For the purpose of comparison, a reference sample (**SWCNT-0**) was prepared by mixing **P-0**—P3HT lacking a Cp end group—with the **p-SWCNT** under identical conditions. Both the **SWCNT-1** and **SWCNT-0** samples were extensively washed with THF—until the washings were colorless—before characterization. The resulting P3HT/SWCNTs covalent hybrid materials were successfully characterized by employing TGA, EA, XPS, and HRTEM.

Thermogravimetric Analysis (TGA). The thermogravimetric profiles of the SWCNT based samples (**p-SWCNT**, **SWCNT-0** and **SWCNT-1**), cyclopentadienyl end-capped P3HT (**P−Cp**) and the nonfunctional P3HT (**P-0**) are depicted in Figure 6.

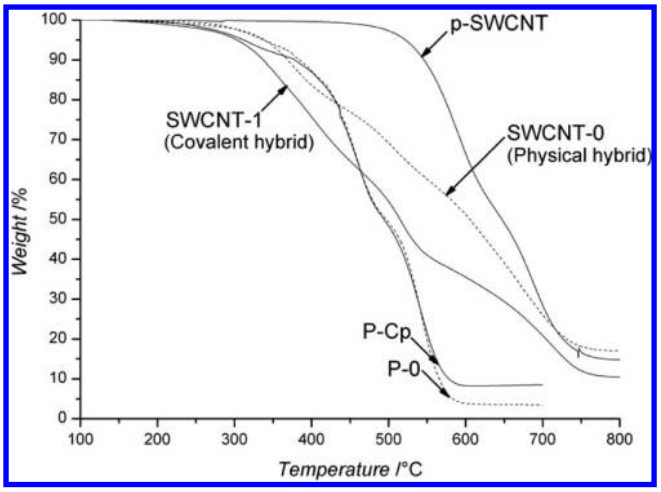

Figure 6. Thermogravimetric profiles of nonmodified SWCNTs (**p-SWCNT**), cyclopentadienyl end-capped P3HT (**P−Cp**), functionalized SWCNTs with **P−Cp** (**SWCNT-1**). Nonfunctional P3HT (**P-0**) and the reference sample SWCNTs mixed with **P-0** (**SWCNT-0**) are represented. A heating rate of 10 °C·min^{-1} was applied, following a 30 min isothermal step at 100 °C.

The analysis of the TGA data was performed by using the first derivative profiles to identify the successive degradation of the samples. Each degradation is characterized by an initial temperature (T_i), a final temperature (T_f), and a temperature corresponding to the maximum rate of weight loss (T_m). In the Supporting Information, the derived profiles are depicted in Figure S9 and a summary of the degradation characteristics is available in Table S1. The nonmodified SWCNTs (**p-SWCNT**) start to decompose at 440 °C until a weight of 14.6% (catalytic residue) at 820 °C. The polymer samples (**P−Cp** and **P-0**) displayed decomposition from 100 to 630 °C in several steps in a similar fashion. At 410 °C, a residual weight of 85.0% for the **P−Cp**, and 85.4% for the **P-0** was observed. A subsequent degradation until 495 °C led both polymers to a similar residual weight percentage, 49.7% for **P−Cp** and 50.4% for **P-0**, before further degradation occurred at higher temperature. The fact that the polymers are not completely degraded before the SWCNTs have started to degrade (T_i = 440 °C) made it difficult to precisely quantify the functionalization of the SWCNTs bonded to P3HT polymer chains. The TGA profiles of the SWCNTs functionalized with the polymer (including the reference sample) revealed the onset of degradation for all the samples at temperatures below T_i (440 °C) of the pristine SWCNTs, evidencing the presence of the polymer in all polymer/SWCNT based samples. Comparing the TGA thermograms of **SWCNT-0** and **SWCNT-1**, one can clearly notice a higher overall weight loss in the case of **SWCNT-1**. The TGA thermograms of the SWCNTs modified with **P−Cp** (**SWCNT-1**), showed a significantly higher degradation when heated to 440 °C (T_i for pristine SWCNTs). For **SWCNT-1**, a weight loss of 37.2% was observed at 440 °C, while at the same temperature a lower weight loss of a weight of 21.8% was observed for **SWCNT-0**. The wrapping of SWCNTs with the P3HT via van der Waals/$\pi-\pi$ interaction accounts for the presence of polymer in **SWCNT-0** samples and most of the P3HT/CNTs hybrid materials reported in literature are based on this physical interaction.[25−27] The onset of SWCNTs degradation before the complete degradation of P3HT made quantification of the grafting density impossible. Nevertheless, the TGA experiments clearly evidenced a higher amount of polymer in case SWCNTs functionalized with Cp end-capped P3HT.

Elemental Analysis (EA). In order to provide complementary information about the presence of the polymer chains for the SWCNTs functionalized or mixed with P3HT, their elemental composition was determined for carbon, hydrogen, nitrogen, oxygen, and sulfur. The results of the elemental analysis are collated in Table 3.

Table 3. Elemental Composition of Non-Modified SWCNTs (p-SWCNT), Cyclopentadienyl End-Capped P3HT (P−Cp), Functionalized SWCNTs with P−Cp (SWCNT-1), and the Reference Samples: Nonfunctional P3HT (P-0) and the SWCNTs Mixed with P-0 (SWCNT-0)[a]

sample	C	H	N	O	S	grafting density /wt %
p-SWCNT	79.1	0.6	0.6	4.1	0	–
P−Cp	69.5	8.2	0.3	0.9	14.3	–
P-0	67.2	7.7	0.4	1.1	14.6	–
SWCNT-1	70.1	2.3	0.9	3.7	3.9	27.3
SWCNT-0	50.9	1.4	0.7	6.9	0.8	8.1

[a]The amount of P3HT incorporated in the hybrid samples expressed as grafting density in wt % is indicated.

For the **p-SWCNT**, the carbon content was found to be 79.1 *wt %* of the composition. Beside carbon, some oxygen (4.1 *wt %*) was also detected. The sum of the percentages of the detected elements (C, H, N, O, S) in the elemental analysis (EA) evidence a missing weight of 15.6% for **p-SWCNT**. As EA is a combustion analysis technique, the 15.6% represents the residual weight and the value is reasonably close to the 14.6% residual weight observed via TGA. We believe that these two values represent the percentage of incombustible impurities in the as-purchased SWCNTs sample. The elemental compositions of **P−Cp** and **P-0** reflected a difference mainly between the carbon, hydrogen, and sulfur atoms, whereas the nitrogen and oxygen contents are not relevant and may be due to air contamination. The compositions also did not exactly

dx.doi.org/10.1021/ma4004055 | *Macromolecules* 2013, 46, 2606−2615

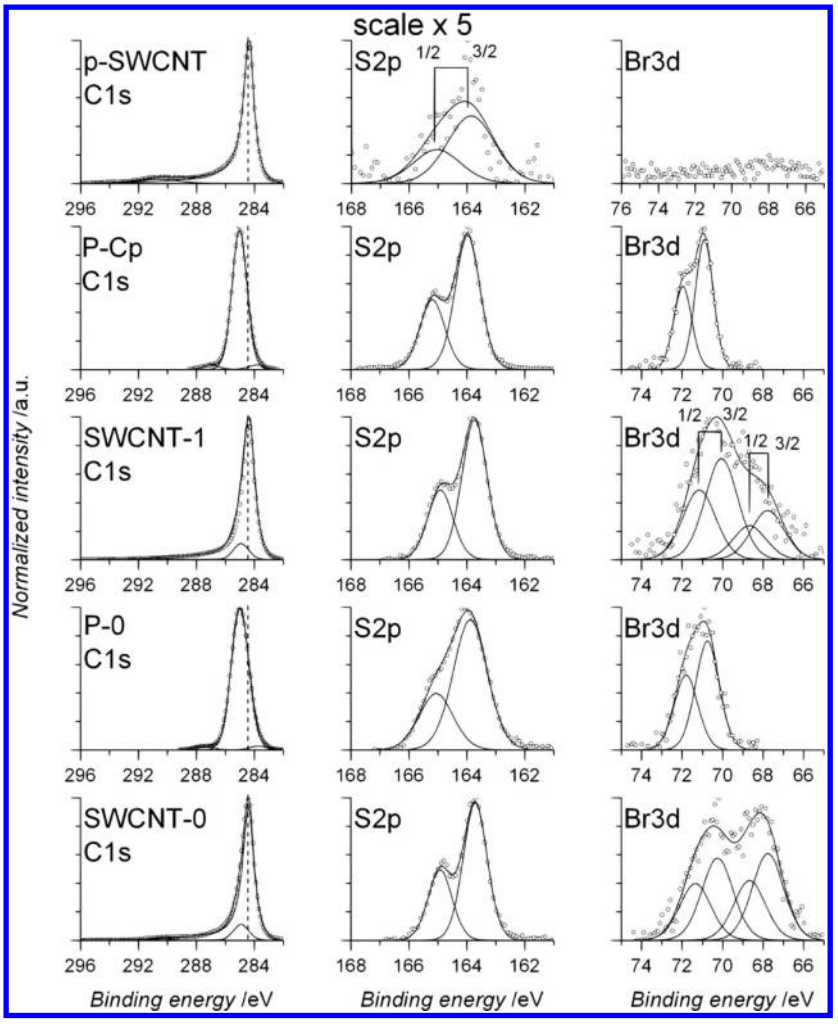

Figure 7. XPS spectra of nonmodified SWCNTs (**p-SWCNT**), cyclopentadienyl end-capped P3HT (**P−Cp**), functionalized SWCNTs with **P−Cp** (**SWCNT-1**). The reference samples, nonfunctional P3HT (**P-0**), and the SWCNTs mixed with **P-0** (**SWCNT-0**) are depicted. For a better visualization, all spectra are normalized to the maximum intensity, and the signal S 2p for **p-SWCNT** is enlarged by a factor of 5.

Table 4. Assignment of Binding Energies and Comparison of the Bond Contribution after the Deconvolution of the XPS Spectra of Non-Modified SWCNTs (p-SWCNT), Cyclopentadienyl End-Capped P3HT (P−Cp), Functionalized SWCNTs with P−Cp (SWCNT-1), and Reference Samples[a]

		at %					
peak	BE[b]/eV	**p-SWCNT**	**P−Cp**	**P-0**	**SWCNT-1**	**SWCNT-0**	entity
Br $3d_{5/2}$	67.7	–	–	–	0.1	0.2	*Br*$^-$
Br $3d_{5/2}$	70.3	–	0.3	0.2	0.2	0.2	*Br*−C
S $2p_{3/2}$	163.9	0.2	8.5	9.2	3.7	2.8	*S*−C
C 1s	283.8	–	2.8	2.4	–	–	$C_{carbide}$
	284.4	93.3	–	–	85.2	85.6	$C-C_{graphite}$
	285.0	–	85.5	85.4	9.9	10.2	C−C, *C*−H
	287.0	–	2.9	2.8	–	–	*C*−*O*, *C*−*Br*
	290.6	6.5	–	–	0.9	1.0	$\pi-\pi^*$

[a]Non-functional P3HT (**P-0**), and the SWCNTs mixed with **P-0** (**SWCNT-0**) are represented. [b]Binding energy.

correspond to the expected theoretical values. The sulfur content is about 5 wt % lower than the theoretical value (see Table S2 in the Supporting Information). For **P-0** and **P−Cp**, the mass balance was not complete. The presence of bromine atoms at the chain end, as evident in the MALDI−TOF MS data discussed earlier, explains the deviation of the experimental EA results from the theoretical values. Bromine, as other halogens, acted as a combustion inhibitor, leading to an incomplete combustion of the sample and to errors in the elemental composition. Quantifying the amount of P3HT polymer chains for **SWCNT-1** and **SWCNT-0** was thus not reliable. However, the analysis of the EA data corroborated the same trend as observed in TGA. First, the sulfur and hydrogen contents increased unambiguously after functionalization with **P−Cp**. The **SWCNT-1** showed sulfur and hydrogen contents of 3.9 and 2.3 *wt %*, respectively. The presence of P3HT was

dx.doi.org/10.1021/ma4004055 | *Macromolecules* 2013, 46, 2606−2615

also observed in **SWCNT-0**, yet in a smaller amount than **SWCNT-1**. The grafting densities in weight percentage (wt %) for the **SWCNT-0** and **SWCNT-1** based samples are presented in the Table 3. Keeping in mind the limitations discussed above (mass balance not complete, presence of bromine as combustion inhibitor) these values must be handled with care. However, one can qualitatively conclude a higher grafting density in case of SWCNTs functionalized with Cp end-capped P3HT as compared to the reference sample where P3HT was physically adsorbed at the surface of SWCNTs.

X-ray Photoelectron Spectroscopy (XPS). Contrary to TGA and EA, which are bulk characterization techniques, XPS offers the possibility to characterize the surface of a sample. Complementary to EA, the elemental composition can also be assessed via XPS. In addition, the same element present in different chemical environments can also be detected. Figure 7 depicts the high resolution XPS scans for the carbon (C 1s), sulfur (S 2p), and bromine (Br 3d) signals obtained for the **p-SWCNT**, **P−Cp**, **SWCNT-1**, **P-0**, and **SWCNT-0**.

The C 1s carbon signal at 284.4 eV is representative the graphitic carbon atoms of **p-SWCNT**.[22b,c] A small amount of sulfur (0.2 at %) was also detected in the case of **p-SWCNT** (refer to Table 4).

XPS spectra for both the polymers (**P−Cp** and **P-0**) showed the presence of bromine, Br $3d_{5/2}$ signal at 70.3 eV,[28,29] originating from the bromo end groups of **P−Cp** and **P-0**. The presence of sulfur signals (S $2p_{3/2}$ signal at 163.9 eV)[30] and the signal for the carbon atoms from hydrocarbon (C 1s signal at 285.0 eV)[31] correlate with the composition of repeat unit for **P−Cp** and **P-0** (3-hexylthiophene-2,5-diyl). A small fraction of the deconvoluted C 1s signal represented by the peak located at 287.0 eV have been assigned to C−Br and C−O.[29] Another small constituting peak of deconvoluted C 1s signal at 283.8 eV could not be attributed unambiguously, however, such a signal is attributable to carbide species which may have originated from contamination.[32] The atomic composition for the carbon, sulfur and bromine contents as determined by XPS are in complete agreement with the theoretical composition for both the polymers (**P−Cp** and **P-0**), reflecting on the higher accuracy of XPS analysis than EA (refer to Table S3 in the Supporting Information section). Like **p-SWCNT**, the C 1s signal for **SWCNT-0** and **SWCNT-1** is dominated by the peak for graphitic carbon at 284.4 eV. The presence of hydrocarbons signals at 285.0 eV reflects on the presence of the P3HT polymer chains in **SWCNT-0** and **SWCNT-1** samples. However, the presence of P3HT in both samples, **SWCNT-1** and **SWCNT-0**, is more evident by the appearance of the signals for sulfur and bromine atoms at the characteristic binding energies of 163.9 eV for S $2p_{3/2}$, and at 67.7 and 70.3 eV for Br $3d_{5/2}$. The results of the elemental composition as determined by XPS are summarized in Table 4. The sulfur content was found to be 3.7 at % for **SWCNT-1**,whereas the sulfur content for **SWCNT-0** was 2.8 at %. The detection of the signal located at 67.7 eV for the Br $3d_{5/2}$ peak may be associated with the formation of bromide ions (Br^-) via decomposition during the XPS analysis.[33] On the basis of similar considerations as in the literature,[22b,c] the amount of atoms (C, H, O, S) introduced from the P3HT chain to the SWCNTs was estimated from the respective atomic percentages (at %). The known molecular weights (M_n) of the polymer samples (**P−Cp** and **P-0**) enabled the estimation of the loading capacity in mmol·g^{-1}. From the theoretical specific area of the SWCNTs (identical to a graphene sheet), the area occupied by the polymer chain at the SWCNT surface can be evaluated in chains·nm^{-2}. The periodicity, i.e. the average number of carbon atoms at the SWCNTs surface per polymer chain, was determined by considering the surface of a hexagonal ring constituted by two residual carbon atoms (each carbon atom being shared between three rings, 6/3 = 2). Table 5 summarizes the grafting density expressed in three different units for **SWCNT-1**. The amount of polymer physically adsorbed at the surface of the reference sample (**SWCNT-0**) is also included in mmol·g^{-1}.

Table 5. Grafting Data Estimated via XPS for the Modified SWCNTs with Cyclopentadienyl End-Capped P3HT (SWCNT-1) and the Reference Sample (SWCNTs Mixed with Nonfunctional P3HT SWCNT-0)

			grafting density		
sample	at %	wt %	mmol·g^{-1}	chain·nm^{-2}	periodicity[a]
SWCNT-1	39.2	46.2	0.111	0.0510	748
SWCNT-0	28.4	32.2	0.0617	–	–

[a]Number of carbon atoms per polymer chain.

As already observed via TGA and EA, the reaction of **P−Cp** with the SWCNTs via Diels−Alder reaction led to a higher amount of polymer grafted at the surface of the SWCNTs. In the **SWCNT-1** sample, the estimated atomic percentage due to the elemental composition of the P3HT chain determined via XPS reads 39.2% and corresponds to a 46.2 wt % of polymer in the sample. The obtained grafting density can be calculated in alternative units, leading to 0.111 mmol·g^{-1} which is equivalent to 0.0510 chain·nm^{-2}. These numbers led to a periodicity of one polymer chain every 748 carbon atoms for **SWCNT-1**. The calculation of such numbers is irrelevant in the case of **SWCNT-0** as the P3HT is only physically adsorbed at the surface of SWCNTs. However, the amount of P3HT adsorbed at the surface of SWCNTs in case of **SWCNT-0** is reported in Table 5 as mmol of P3HT per gram of SWCNTs. A comparison of the data provided in Table 5 revealed that the amount of polymer in **SWCNT-1** sample was 2 times higher than the reference sample **SWCNT-0**. The analysis thus confirmed the efficient grafting of P3HT at the surface of the SWCNTs via Diels−Alder reaction employing cyclopentadienyl end-capped P3HT polymer compared to the physical wrapping effect in case of the reference sample. Compared to the loading capacity obtained for the SWCNTs surface functionalization with the Cp end-capped poly(methyl)methacrylate (0.064 to 0.086 mmol·g^{-1} for M_n 2900 g·mol^{-1}) and poly(*N*-isopropyl)-acrylamide (0.0520 to 0.0628 mmol·g^{-1} for M_n 5400 g·mol^{-1}),[22b,c] the loading capacity observed for **P−Cp** is 2 times higher (0.111 mmol·g^{-1}). A comparatively higher supramolecular affinity between P3HT and SWCNTs can lead to an enhanced proximity of reactive Cp end groups to the surface of SWCNTs which may account for the higher grafting density in case of **P−Cp**.

In order to further characterize and differentiate the reference sample **SWCNT-0** from **SWCNT-1**, the samples were analyzed with HRTEM.

High Resolution Transmission Electron Microscopy (HRTEM). Figure 8 depicts representative HRTEM images of the nonmodified SWCNTs (top, left side, **p-SWCNT**), the SWCNTs functionalized with cyclopentadienyl end-capped P3HT (top, right side, **SWCNT-1**) and the reference sample

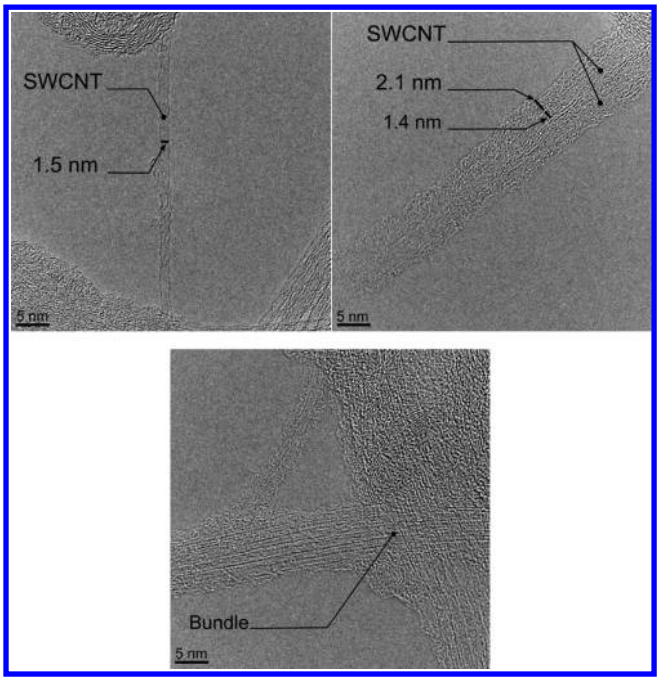

Figure 8. HRTEM images of nonmodified SWCNTs (**p-SWCNT**, top, left), SWCNTs functionalized with **P−Cp** (**SWCNT-1**, top right side), and the reference sample of SWCNTs mixed with nonfunctional P3HT **P-0** (**SWCNT-0**, bottom).

(SWCNTs mixed with nonfunctional P3HT, bottom, **SWCNT-0**).

The single-walled nature of the SWCNTs was observed in all cases, with a tube diameter ranging between 1.0 and 1.6 nm. The **p-SWCNT** expectedly exhibited a surface free from any amorphous carbon. In the case of **SWCNT-1**, the surface of the individual SWCNTs was covered by an amorphous layer (thickness estimated by 2.1 nm) of P3HT polymer. The amorphous layer of P3HT was also found wrapping the SWCNTs in the reference sample **SWCNT-0**; however, in case of the **SWCNT-0** the sample was predominantly constituted by bundles of SWCNTs wrapped by the amorphous P3HT. On the other hand, microscopic agglomerates were detected in **SWCNT-0** which appeared to be coated with the polymer film (refer to Figure S10 in Supporting Information). Beside those aggregates the polymer layer also appeared to have covered the whole copper grid, which led to critical conditions for the HRTEM observation. Such a behavior of the reference sample suggests that the nonfunctional P3HT may be initially physisorbed at the surface of the SWCNTs, but the subsequent ultrasonic treatment for the HRTEM sample preparation resulted in the desorption of the polymer chains from the surface of the SWCNTs, leading to a polymer film covering the copper grid. A UV/vis spectroscopic analysis of the chloroform extract after ultrasonication of both samples (**SWCNT-0** and **SWCNT-1**) underpins the covalently bonded nature of the P3HT in the **SWCNT-1** sample, as substantial amounts of P3HT leached from the **SWCNT-0** sample and only limited P3HT leaching was observed in the chloroform extract of **SWCNT-1**. The UV/vis absorption spectra after sonification evidence that the amount of detached P3HT is substantially lower in the **SWCNT-1** sonicated sample compared to the **SWCNT-0** sample (refer to Figure S11 in the Supporting Information). A combination of some ultrasound assisted retro DA reaction[34] and slight physisorption of polymer in addition to the covalent grafting accounts for the P3HT observed in the chloroform extract of **SWCNT-1**. Contrary to the **SWCNT-0**, the **SWCNT-1** sample did not display any aggregation during the HRTEM analysis, highlighting the effective debundling of SWCNTs by covalent grafting of polymer chains at the surfaces of the SWCNTs via the Diels−Alder reaction between the Cp terminus of the P3HT polymer and surface of the SWCNTs. Furthermore, the covalent attachment resulted in a stable dispersion of **SWCNT-1** in chloroform without any sign of aggregation over a period of 5 days whereas the dispersion of **SWCNT-0** in chloroform showed a clear aggregation after 12 h (refer to Figure S12 in the Supporting Information).

CONCLUSIONS

We have demonstrated—for the first time—the scope of the Diels−Alder reaction between Cp capped P3HT and SWCNTs surface as a facile mean for covalent functionalization of SWCNTs with conducting P3HT polymer. *In situ* end group capping using the GRIM method and subsequent end group transformations led to the unprecedented Cp capped P3HT. The reaction of an aliphatic bromo group terminated P3HT with $NiCp_2$ selectively and quantitative transformed only the terminal aliphatic bromo group into the Cp group. The inertness of bromo groups directly attached to the thiophene ring exclusively led to P3HT with Cp groups only at one end of polymer chain. The terminal Cp groups were reactive toward dithioester based dienophiles under HDA reaction conditions, which was demonstrated by the preparation of a P3HT-*b*-PS block copolymer. The DA ligation of Cp-terminated P3HT produced P3HT/SWCNTs molecular hybrid materials, where individual SWCNTs were functionalized with P3HT, thus addressing the bundling issue intrinsically associated with CNTs. The presented synthetic strategy holds substantial promise for generating OCP- and CNTs-based novel materials for a wide range of applications.

ASSOCIATED CONTENT

Supporting Information

Materials and instruments used, synthesis of **P-0**, **P-Vinyl**, **P−OH**, and **P−Br**, their ^{1}H NMR and MALDI−TOF mass spectra, comparison of simulated and experimentally determined mass spectra, ^{1}H NMR spectra of P3HT-*b*-PS, DTGA data, EA data, TEM images of aggregates, UV/vis spectra, and digital photographs of the dispersions of **SWCNT-1** and **SWCNTs-0** in $CHCl_3$. This material is available free of charge via the Internet at http://pubs.acs.org.

AUTHOR INFORMATION

Corresponding Author

*E-mail: christopher.barner-kowollik@kit.edu. Telephone: +49 721 608-45641. Fax: +49 721 608-45740.

Notes

The authors declare no competing financial interest.

ACKNOWLEDGMENTS

B.Y. thanks the Alexander von Humboldt Foundation for financial support via a Georg Forster Research Fellowship for Postdoctoral Researchers. C.B.-K. acknowledges continued funding from the German Research Council (DFG), the Fraunhofer ICT and the Karlsruhe Institute of Technology (KIT) as well as the Ministry of Science and Arts of the state of Baden-Württemberg.

REFERENCES

(1) (a) Oberlin, A.; Endo, M.; Koyama, T. *J. Cryst. Growth* **1976**, *32*, 335−349. (b) Iijima, S. *Nature* **1991**, *354*, 56−58. (c) Baughman, R.; Zakhidov, A. A.; de Heer, W. A. *Science* **2002**, *297*, 787−792. (d) Ellmer, K. *Nat. Photonics* **2012**, *6*, 808−816. (e) Zheludev, N. I.; Kivshar, Y. S. *Nat. Mater.* **2012**, *11*, 917−924. (f) Lu, W.; Zu, Me; Byun, J.-H.; Kim, B.-S.; Chou, T.-W. *Adv. Mater.* **2012**, *24*, 1805−1833. (i) Gao, C.; Guo, Z.; Liu, J.-H.; Huang, X.-J. *Nanoscale* **2012**, *4*, 1948−1963. (j) Meng, L.; Zhang, X.; Lu, Q.; Fei, Z.; Dyson, P. J. *Biomaterials* **2012**, *33*, 1689−1698. (k) Liu, Y.; Dong, X.; Chen, P. *Chem. Soc. Rev.* **2012**, *41*, 2283−2307. (l) Huang, H.; Yuan, Q.; Shah, J. S.; Misra, R. D. K. *Adv. Drug Delivery Rev.* **2011**, *63*, 1332−1339.

(2) Girifalco, L. A.; Hodak, M.; Lee, R. S. *Phys. Rev. B: Condens. Matter* **2000**, *62*, 13104−13110.

(3) (a) Sahoo, N. G.; Rana, S.; Cho, J. W.; Li, L.; Chan, S. H. *Prog. Polym. Sci.* **2010**, *35* (7), 837−867. (b) Qian, H.; Greenhalgh, E. S.; Shaffer, M. S. P.; Bismarck, A. *J. Mater. Chem.* **2010**, *20*, 4751−4762. (c) Spitalsky, Z.; Tasis, D.; Papagelis, K.; Galiotis, C. *Prog. Polym. Sci.* **2010**, *35* (3), 357−401. (d) Moniruzzaman, M.; Winey, K. I. *Macromolecules* **2006**, *39* (16), 5194−5205. (e) Bekyarova, E.; Itkis, M. E.; Cabrera, N.; Zhao, B.; Yu, A. P.; Gao, J.; Haddon, R. C. *J. Am. Chem. Soc.* **2005**, *127*, 5990−5995.

(4) (a) Chen, J.; Hamon, M. A.; Hu, H.; Chen, Y. S.; Rao, A. M.; Eklund, P. C.; Haddon, R. C. *Science* **1998**, *282*, 95−98. (b) Tasis, D.; Tagmatarchis, N.; Bianco, A.; Prato, M. *Chem. Rev.* **2006**, *106*, 1105−1136. (c) Banerjee, S.; Hemraj-Benny, T.; Wong, S. *Adv. Mater.* **2005**, *17*, 17−19. (d) Hirsch, A. *Angew. Chem., Int. Ed.* **2002**, *41*, 1853−1859.

(5) (a) Nelson, J. *Curr. Opin. Solid State Mater. Sci.* **2002**, *6*, 87−95. (b) Pivrikas, A.; Sariciftci, N. S.; Juska, G.; Osterbacka, R. *Prog. Photovoltaics* **2007**, *15*, 677−696. (c) Turner, J. A. *Science* **1999**, *285*, 687−689. (d) Whitesides, G. M.; Crabtree, G. W. *Science* **2007**, *315*, 796−798. (e) Szuromi, P.; Jasny, B.; Clery, D.; Austin, J.; Hanson, B. *Science* **2007**, *315*, 781. (f) Lewis, N. *Science* **2007**, *315*, 798−801. (g) Shah, A. *Science* **1999**, *285*, 692−698.

(6) Sgobba, V.; Guldi, D. M. *Chem. Soc. Rev.* **2009**, *38*, 165−184.

(7) (a) Carlson, D. E.; Wronski, C. R. *Appl. Phys. Lett.* **1976**, *28*, 671−673. (b) Naghavi, N.; Spiering, S.; Powalla, M.; Cavana, B.; Lincot, D. *Prog. Photovoltaics* **2003**, *11*, 437−443. (c) O'Regan, B.; Grätzel, M. *Nature* **1991**, *353*, 737−740. (e) Huynh, W.; Dittmer, J.; Alivisatos, A. P. *Science* **2002**, *295*, 2425−2427.

(8) (a) Holt, J.; Singh, S.; Drori, T.; Zhang, Y.; Vardeny, Z. V. *Phys. Rev. B* **2009**, *79*, 195−210.

(9) (a) Yu, D.; Yang, Y.; Durstock, M.; Baek, J.-B.; Dai, L. *ACS Nano* **2010**, *4*, 5633−5640. (b) Araújo, G.; Arantes, C.; Roman, L. S.; Zarbin, A. J. G.; Rocco, M. L. M. *Surf. Sci.* **2009**, *603*, 647−652.

(10) Liang, Y.; Xu, Z.; Xia, J.; Tsai, S.-T.; Wu, Y.; Li, G.; Ray, C.; Yu, L. *Adv. Energy Mater.* **2010**, *22*, E135−E138.

(11) Radbeh, R.; Parbaile, E.; Chakaroun, M.; Ratier, B.; Aldissi, M.; Moliton, A. *Polym. Int.* **2010**, *59*, 1514−1519.

(12) (a) Kanai, Y.; Grossman, J. C. *Nano Lett.* **2008**, *8*, 908−912. (b) Stranks, S. D.; Weisspfennig, C.; Parkinson, P.; Johnston, M. B.; Herz, L. M.; Nicholas, R. J. *Nano Lett.* **2011**, *11*, 66−72. (c) Ren, S.; Bernardi, M.; Lunt, R. R.; Bulovic, V.; Grossman, J. C.; Gradečak, S. *Nano Lett.* **2011**, *11*, 5316−5321.

(13) Chen, R. J.; Zhang, Y.; Wang, D.; Dai, H. *J. Am. Chem. Soc.* **2001**, *123*, 3838−3839.

(14) Kuila, B. K.; Park, K.; Dai, L. *Macromolecules* **2010**, *16*, 6699−6705.

(15) Kumar, N. A.; Kim, S. H.; Cho, B. G.; Lim, K. T.; Jeong, Y. T. *Colloid Polym. Sci.* **2009**, *287*, 97−102.

(16) Boon, F.; Desbief, S.; Cutaia, L.; Douhéret, O.; Minoia, A.; Ruelle, B.; Clément, S.; Coulembier, O.; Cornil, J.; Dubois, P.; Lazzaroni, R. *Macromol. Rapid Commun.* **2010**, *31*, 1427−1434.

(17) Niu, L.; Li, P.; Chen, Y.; Wang, J.; Zhang, J.; Zhang, B.; Blau, W. J. *J. Polym. Sci., Part A: Poly. Chem.* **2011**, *49*, 101−109.

(18) Sadhu, V.; Nismy, N. A.; Adikaari, A. A. D. T.; Henley, S. J.; Shkunov, M.; Silva, S. R. P. *Nanotechnology* **2011**, *22*, 265607−265611.

(19) Phuong, A.; Huang, T.-M.; Chen, P.-T.; Yang, A. C.-M. *J. Polym. Sci., Part B: Polym. Phys.* **2011**, *49*, 581−590.

(20) Hauke, F.; Hirsch, A. *Covalent Functionalization of Carbon Nanotubes, in Carbon Nanotubes and Related Structures: Synthesis, Characterization, Functionalization, and Applications*; Guldi, D. M., Martín, N., Eds.; Wiley-VCH Verlag GmbH & Co. KGaA: Weinheim, Germany, 2010; doi: 10.1002/9783527629930.ch6.

(21) (a) Sinnwell, S.; Inglis, A. J.; Davis, T. P.; Stenzel, M. H.; Barner-Kowollik, C. *Chem. Commun.* **2008**, 2052−2054. (b) Nebhani, L.; Sinnwell, S.; Inglis, A. J.; Stenzel, M. H.; Barner-Kowollik, C.; Barner, L. *Macromol. Rapid Commun.* **2008**, *29*, 1431−1437. (c) Inglis, A. J.; Stenzel, M. H.; Barner-Kowollik, C. *Macromol. Rapid Commun.* **2009**, *30*, 1792−1798. (d) Inglis, A. J.; Sinnwell, S.; Stenzel, M. H.; Barner-Kowollik, C. *Angew. Chem., Int. Ed.* **2009**, *48*, 2411−2414. (e) Nebhani, L.; Sinnwell, S.; Lin, C. Y.; Coote, M.; Stenzel, M. H.; Barner-Kowollik, C. *J. Polym. Sci., Part A: Polym. Chem.* **2009**, *47*, 6053−6071. (f) Pauloehrl, T.; Inglis, A. J.; Barner-Kowollik, C. *Adv. Mater.* **2010**, *22*, 2788−2791. (g) Nebhani, L.; Schmiedl, D.; Barner, L.; Barner-Kowollik, C. *Adv. Funct. Mater.* **2010**, *20*, 2010−2020. (h) Inglis, A. J.; Pauloehrl, T.; Barner-Kowollik, C. *Macromolecules* **2010**, *43*, 33−36.

(22) (a) Nebhani, L.; Barner-Kowollik, C. *Macromol. Rapid Commun.* **2010**, *31*, 1298−1305. (b) Zydziak, N.; Hübner, C.; Bruns, M.; Barner-Kowollik, C. *Macromolecules* **2011**, *44*, 3374−3380. (c) Zydziak, N.; Hübner, C.; Bruns, M.; Vogt, A. P.; Barner-Kowollik, C. *Polym. Chem.* **2013**, *4*, 1525−1537.

(23) (a) Lu, X.; Tian, F.; Wang, N.; Zhang, Q. *Org. Lett.* **2002**, *24*, 4313−4315. (b) Chang, C.-M.; Liu, Y.-L. *Carbon* **2009**, *47*, 3041−3049. (c) Mercuri, F.; Sgamellotti, A. *Phys. Chem. Chem. Phys.* **2009**, *11*, 563−567. (d) McPhail, M. R.; Sells, J. A.; He, Z.; Chusuei, C. C. *J. Phys. Chem. C* **2009**, *113*, 14102−14109. (e) Paiva, M. C.; Xu, W.; Proença, M. F.; Novais, R. M.; Lægsgaard, E.; Besenbacher, F. *Nano Lett.* **2010**, *10*, 1764−1768. (f) Zhang, W.; Sprafke, J. K.; Ma, M. L.; Tsui, E. Y.; Sydlik, S. A.; Rutledge, G. C.; Swager, T. M. *J. Am. Chem. Soc.* **2009**, *131*, 8446−8454.

(24) (a) Iovu, M. C.; Jeffries-El, M.; Sheina, E. E.; Cooper, J. R.; McCollough, R. D. *Polymer* **2005**, *46*, 8582−8586. (b) Jeffries-El, M.; Sauvé, G.; McCullough, R. D. *Macromolecules* **2005**, *38*, 10346−10352. (c) Jeffries-El, M.; Sauvé, G.; McCullough, R. D. *Adv. Mater.* **2004**, *16*, 1017−1019.

(25) Giulianini, M.; Waclawik, E. R.; Bell, J. M.; De Crescenzi, M.; Castrucci, P.; Scarselli, M.; Motta1, N. *Appl. Phys. Lett.* **2009**, *95*, 013304−013306.

(26) Bernardi, M.; Giulianini, M.; Grossman, J. C. *ACS Nano* **2010**, *4*, 6599−6606.

(27) Caddeo, C.; Melis, C.; Colombo, L.; Mattoni, A. *J. Phys. Chem. C* **2010**, *114*, 21109−21113.

(28) Matrab, T.; Chehimi, M. M.; Pinson, J.; Slomkowski, S.; Basinska, T. *Surf. Interface Anal.* **2006**, *38*, 565−568.

(29) Yuan, S.; Wan, D.; Liang, B.; Pehkonen, S. O.; Ting, Y. P.; Neoh, K. G.; Kang, E. T. *Langmuir* **2011**, *27*, 2761−2774.

(30) Joseph, Y.; Besnard, I.; Rosenberger, M.; Guse, B.; Nothofer, H.-G.; Wessels, J. M.; Wild, U.; Knop-Gericke, A.; Su, D.; Schloegl, R.; Yasuda, A.; Vossmeyer, T. *J. Phys. Chem. B* **2003**, *107*, 7406−7413.

(31) Lock, E. H.; Petrovykh, D. Y.; Mack, P.; Carney, T.; White, R. G.; Walton, S. G.; Fernsler, R. F. *Langmuir* **2010**, *26*, 8857−8868.

(32) Bruns, M.; Geckle, U.; Trouillet, V.; Rudolphi, M.; Baumann, H. *J. Vac. Sci. Technol. A* **2005**, *23*, 1114−1119.

(33) (a) Al-Bataineh, S. A.; Britcher, L. G.; Griesser, H. J. *Surf. Sci.* **2006**, *600*, 952−962. (b) Al-Bataineh, S. A.; Britcher, L. G.; Griesser, H. J. *Surf. Interface Anal.* **2006**, *38*, 1512−1518.

(34) Wiggins, K. M.; Syrett, J. A.; Haddleton, D. M.; Bielawski, C. W. *J. Am. Chem. Soc.* **2011**, *133*, 7180−7189.